IEEE Access
Multidisciplinary | Rapid Review | Open Access Journal

Received November 10, 2019, accepted December 10, 2019, date of publication December 16, 2019,
date of current version December 31, 2019.

Digital Object Identifier 10.1109/ACCESS.2019.2959944

Study on the Compatibility of Multi-Bifurcations by Simulations of Pattern Formation

FEIFAN ZHANG, XUANWEN WU, WENJIAO ZHOU, LEI YAO, AND HUAYONG ZHANG
Research Center for Engineering Ecology and Nonlinear Science, North China Electric Power University, Beijing 102206, China

Corresponding author: Huayong Zhang (rceens@ncepu.edu.cn)

This work was supported in part by the Major Science and Technology Program for Water Pollution Control and Treatment under Grant 2017ZX07101003-06, and in part by the National Natural Science Foundation of China under Grant 11875126 and Grant 11771140.

ABSTRACT Bifurcation is considered the main mathematical mechanism for the formation of spatial self-organizing patterns in many studies. When bifurcation was initially defined, only the transition of the system from stable state to unstable state or from uniform state to non-uniform state was concerned, without considering the compatibility of each bifurcation. The coupling phenomenon between bifurcations can be deduced from the characteristics of bifurcation pattern and pattern type. In this paper, we choose a classical wind-sand vegetation model as an example to study the compatibility between bifurcations. Firstly we transformed the vegetation-sand model into a discrete model to study its fixed point and stability analysis. Then we researched the dynamics of the three bifurcations of Flip bifurcation, Neimark-Sacker bifurcation, Turing bifurcation and their mutual coupling. The numerical simulation of the parameters of the three kinds of bifurcations is carried out, and the bifurcation points are simulated on the basis of bifurcation conditions. The simulation results show that both Flip bifurcation, Neimark-Sacker bifurcation and Turing bifurcation can produce complex vegetation patterns, and the coupling effects of any two types of bifurcation can also produce self-organization. The results of this paper will provide support for the improvement of bifurcation definition in the future work.

INDEX TERMS Flip bifurcation, Neimark-Sacker bifurcation, Turing bifurcation, pattern self-organization.

I. INTRODUCTION

Bifurcation is an important reason for the formation of self-organizing patterns [1]–[4]. In recent years, many studies have taken bifurcation as the main mathematical mechanism for the forming spatial self-organizing patterns, and have obtained simulated patterns that are highly similar to the actual patterns [5], [6]. It can be said that pattern and bifurcation have been very closely linked. There are various kinds of bifurcation, such as Turing, Hopf, Neimark-Sacker, Flip. Each bifurcation can lead to the production of patterns of specific types. For example, generally speaking, Turing bifurcation can be produced [7]–[9]. From the type of partial pattern, it looks like the result of multiple bifurcations. However, from the definition of bifurcation, the bifurcations conflict with each other and cannot be superimposed. This is because, in the initial definition of bifurcation, only the transition of the system from stable state to unstable state or from uniform state to non-uniform state is concerned, without considering the compatibility of various bifurcations. Although coupling between bifurcations can hardly be explained from the definition of bifurcation, it can be inferred from the above by the characteristics of bifurcation graphs and pattern types.

Wind-sand vegetation pattern is a kind of large-scale pattern with very high visualization degree. In this paper, we choose a wind-sand vegetation model as an example to study the compatibility between bifurcations. Zhang et al. [10] proposed a vegetation-sand model using partial differential equations to interpret the mechanism of vegetation self-organization in windy sandy environments [11]–[15]. Vegetation patterns have been widely observed in arid and semi-arid areas, there have been many studies on the exploration of pattern self-organization mechanisms [16]. The research of vegetation patterns is mainly based on the establishment of theoretical model [17]. The continuous vegetation-sand model was proposed by [10] and is shown as:

$$\frac{\partial S}{\partial t} = k_0 + mV\left(1 - \frac{V}{V_0}\right) - nS - a_1\frac{\partial S}{\partial x} + D_1\left(\frac{\partial^2 S}{\partial x^2} + \frac{\partial^2 S}{\partial y^2}\right),$$

The associate editor coordinating the review of this manuscript and approving it for publication was Chao-Yang Chen.

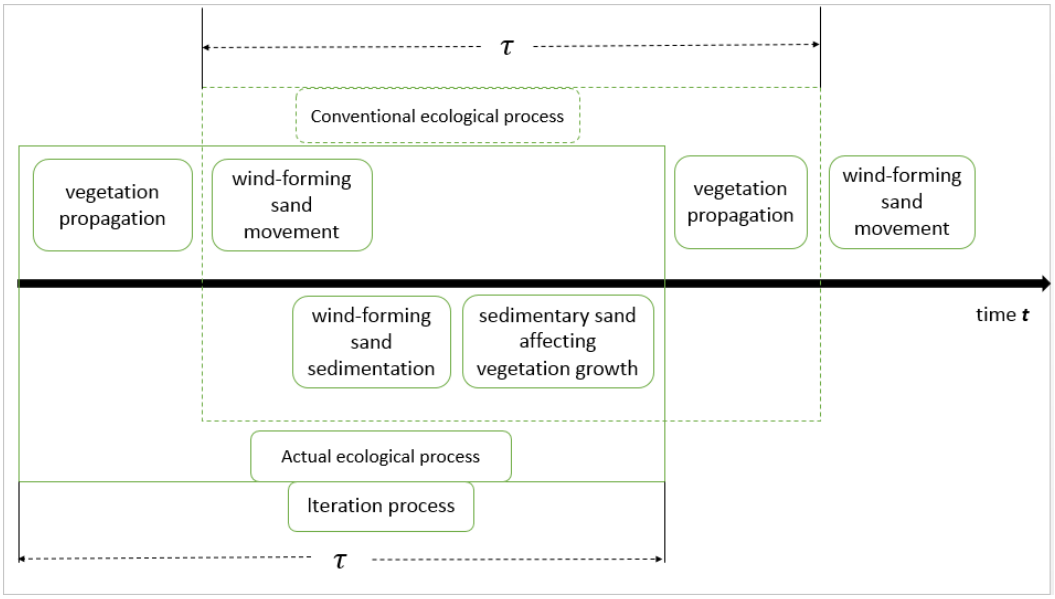

FIGURE 1. Orders of ecological processes in reality and in the iterations.

$$\frac{\partial V}{\partial t} = hV\left(1 - \frac{V}{V_m}\right) - pS\frac{V}{C+V} - a_2\frac{\partial V}{\partial x} + D_2\left(\frac{\partial^2 V}{\partial x^2} + \frac{\partial^2 V}{\partial y^2}\right) \tag{1.1}$$

Here $S(cm)$ represents the height of sand deposition. Parameter $k_0\left(cm \cdot d^{-1}\right)$ is the accumulation rate of air sand without vegetation. $m\left(cm \cdot d^{-1}\right)$ is the coefficient representing the trapping effect of vegetation. Parameters k_0 and m are affected by sand flow intensity. The trapping effects of vegetation decrease with the increase of vegetation cover until a certain value (near 100%) of vegetation cover (saturation constant of vegetation trapping effects), and $V_0\,(\%)$ is two times of this certain value. $n\left(d^{-1}\right)$ is the coefficient representing the decrease of accumulation rate with the increase of sand height. $a_1\left(m \cdot d^{-1}\right)$ is the coefficient representing the translation of sand dunes by wind. $D_1\left(m^2 \cdot d^{-1}\right)$ is the diffusion coefficient of sand without strong unidirectional wind. $V\,(\%)$ represents vegetation coverage, and $h\left(d^{-1}\right)$ represents the intrinsic growth rate of vegetation. $V_m(\%)$ is the potential maximum of vegetation coverage. $p\left(cm \cdot d^{-1}\right)$ is the coefficient of destruction effect by sand. $C(\%)$ is a constant representing how sand tolerance increases with the increase of vegetation cover. $a_2\left(m \cdot d^{-1}\right)$ is the advection coefficient representing the dispersal of vegetation by wind. $D_2\left(m^2 \cdot d^{-1}\right)$ is the diffusion coefficient representing the dispersal of vegetation without strong unidirectional wind. x and y are space axes, and t is time. The values and meanings of the parameters are referenced in [10]. Wind direction is along the positive x direction. When there is no prevailing wind, the effects of wind are modeled as diffusion terms. When there is a prevailing wind, its effects can be modeled by adding an advection term to the diffusion terms as shown in model (1).

In the model of this paper, the spatial diffusion and flow processes of vegetation and sedimentary sand are considered first. Then we consider the reaction process of vegetation and sedimentary sand itself (including the interaction between vegetation and sedimentary sand). The four ecological processes shown in Figure 1 are in accordance with the speed of their occurrence, in the order of time: wind-forming sand movement, wind-forming sand sedimentation, sedimentary sand affecting vegetation growth, and vegetation propagation (see the dotted line in Figure 1). The movement of wind-forming sand is faster than the growth of vegetation, so the change of wind-forming sand is ahead. In Figure 1, these four processes are defined as regular ecological processes and cycle through time.

In the discrete model (2.1) of this paper, focusing on the intrinsic growth rate of vegetation $h\left(d^{-1}\right)$, Flip bifurcation and Neimark-Sacker bifurcation can occur without spatial terms. Neimark-Sacker bifurcation is one of the most important bifurcations in discrete dynamics. Through Neimark-Sacker bifurcation, the stable state of system bifurcates from a fixed point to an invariant circle. It should be noted that with spatial terms such as advection and diffusion, Turing bifurcation can also occur. Naturally, a question arises as to what the dynamics will be can Turing-Flip, Turing-Neimark-Sacker, Flip-Neimark-Sacker and Turing-Neimark-Sacker-Flip bifurcation occurs, and how they influence the self-organization of vegetation patterns.

In this paper, we transform the vegetation-sand model [17] to a spatially and temporally discrete model. Then, focusing on the stable fixed point, bifurcation analysis including Flip bifurcation, Neimark-Sacker bifurcation and Turing bifurcation will be carried out. Bifurcation diagram and phase portrait will be shown. Based on bifurcation analysis, we can select parameter values around each bifurcation. Given these

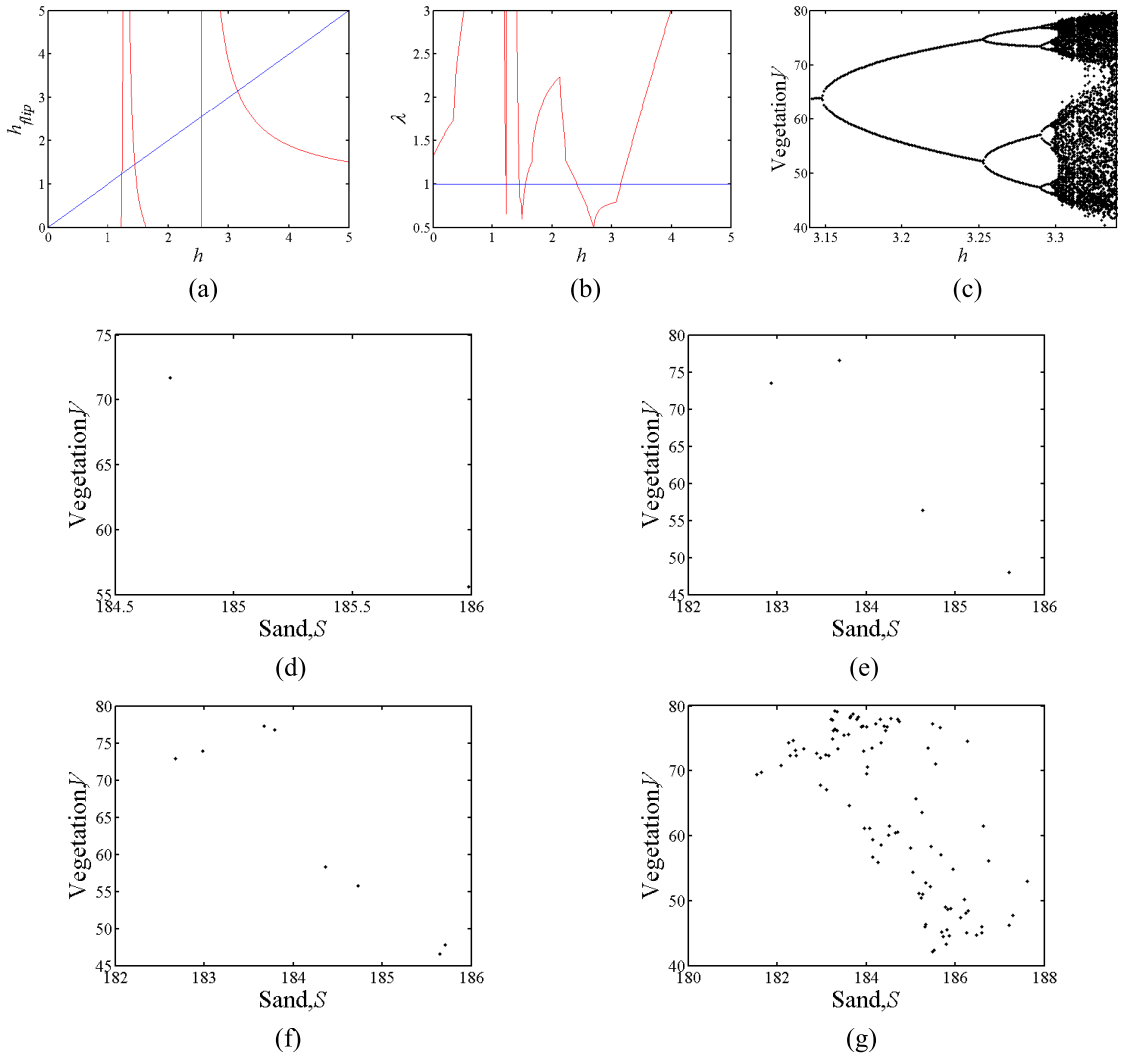

FIGURE 2. Solving the critical point, Bifurcation diagram, Eigenvalue function graph and phase portraits of flip bifurcation. (a) The red curve is h_{flip} (h) and the blue curve is h; (b) The red curve is λ (h) and the blue curve is λ = 1; (c) Bifurcation diagram with parameters: $m = 0.2$; $n = 0.07$; $\tau = 2$; $p = 0.45$; $k_0 = 4.36$; $V_m = 100\%$; $V_0 = 200\%$; $C = 10\%$; (d–g) Phase portraits with parameter (d) $h = 3.2$; (e) $h = 3.28$; (f) $h = 3.293$; (g) $h = 3.327$.

parameters, simulations will be carried out to show how patterns form. A variety of patterns we can get. Finally, we will discuss the possible reasons that cause the different pattern.

II. MODEL AND BIFURCATION ANALYSIS

For certain deterministic nonlinear systems, when a certain parameter of the system changes to a critical value, the global properties (qualitative properties, topological properties, etc.) of the system will suddenly change, which is called bifurcation phenomenon. Bifurcation is a very important dynamic phenomenon in nonlinear systems. In the field of vegetation pattern study, most researches apply Turing bifurcation theory to explain the symmetry breaking behavior during pattern formation. Turing bifurcation cause spatial symmetry fractures, resulting in the formation of temporally fixed and spatially oscillating patterns [16]. In this study, Turing bifurcation is applied to study the mechanism of vegetation pattern formation in spatio-temporal discrete difference model. A large number of research results in other pattern fields show that more complex dynamic behaviors and richer pattern types can be formed under various bifurcation dynamics [18]–[21]. When temporal and spatial symmetry breaking occur simultaneously, the discrete model will generate patterns that oscillate both spatially and temporally. In this section, the parameter conditions of Flip bifurcation, Flip-Turing bifurcation and both bifurcations will be obtained.

A. A DISCRETE VEGATATION-SAND MODEI

Previous researches on discrete dynamic system [22]–[30] have laid a solid theoretical foundation for this paper to analyze the dynamic behavior of spatial-temporal discrete vegetation-sand model. In this research, the above continuous model will be transformed to a discrete model (2.1). We consider the model on a $N \times N$ lattice,

and the two variables can be expressed as $S(i,j,t)$ and $V(i,j,t)$ $\left(i,j \in \{1,2,3,\ldots,N\}\right.$ and $\left.t \in Z^{+}\right)$, that represent the height of sand deposition and the vegetation coverage in lattice (i,j) at time t, respectively. According to the former research works of [13], [26]–[28], there are two stages, reaction stage and diffusion stage, when we discretize the continuous model (1.1). The spatial dispersal stage, that are advection and diffusion, is considered firstly as:

$$\begin{cases} S'_{(i,j,t)} = S_{(i,j,t)} + \dfrac{\tau}{d} a_1 \nabla_d S_{(i,j,t)} + \dfrac{\tau}{d^2} D_1 \nabla_d^2 S_{(i,j,t)} \\ V'_{(i,j,t)} = V_{(i,j,t)} + \dfrac{\tau}{d} a_2 \nabla_d V_{(i,j,t)} + \dfrac{\tau}{d^2} D_2 \nabla_d^2 V_{(i,j,t)} \end{cases} \tag{2.1a}$$

$$\begin{cases} S_{(i,j,t+1)} = S'_{(i,j,t)} + \tau \left(k_0 + m V'_{(i,j,t)} \left(1 - \dfrac{V'_{(i,j,t)}}{V_0} \right) - n S'_{(i,j,t)} \right) \\ V_{(i,j,t+1)} = V'_{(i,j,t)} + \tau \left(h V'_{(i,j,t)} \left(1 - \dfrac{V'_{(i,j,t)}}{V_m} \right) - p S'_{(i,j,t)} \dfrac{V'_{(i,j,t)}}{C + V'_{(i,j,t)}} \right) \end{cases} \tag{2.1b}$$

where τ and d are the time step and space step respectively. ∇_d denotes the discrete form of advections. ∇_d^2 denotes the discrete form of the Laplacian operator. Boundary conditions are set as periodic conditions.

B. FLIP BIFURCATION ANALYSIS

Assume that $U_0(\mu)$is the asymptotically stable fixed points of map:

$$U_0 \to F(U_0, \mu), \quad U_0 \in R^2, \ \mu \in R^1 \tag{2.2}$$

Let the fixed point of mapping (2.2) at $\mu = \mu_0$ be U_0 and its corresponding eigenvalue be 1. If the following conditions are met,

$$\begin{aligned} \frac{\partial F_1}{\partial \mu} \frac{\partial^2 F_1}{\partial U_1^2} + 2 \frac{\partial^2 F_1}{\partial U_1 \partial \mu} &= \frac{\partial F_1}{\partial \mu} \frac{\partial^2 F_1}{\partial U_1^2} - \left(\frac{\partial F_1}{\partial U_1} - 1 \right) \frac{\partial^2 F_1}{\partial U_1 \partial \mu} \\ &\neq 0, \\ (U_1, \mu) &= (U_0, \mu_0) \end{aligned} \tag{2.3}$$

$$\begin{aligned} a &= \frac{1}{2} \left(\frac{\partial^2 F_1}{\partial U_1^2} \right)^2 + \frac{1}{3} \frac{\partial^3 F_1}{\partial U_1^3} \neq 0, \\ (U_1, \mu) &= (U_0, \mu_0) \end{aligned} \tag{2.4}$$

So the map (2.2) bifurcates periodically at the fixed point (U_0, μ_0) and produces a 2-period orbital.

According to the Flip bifurcation condition [34]: $\lambda = -1$. So $\Delta = -tr(J) - 1$, in which

$$\begin{aligned} \Delta &= det(J) = h_A h + h_B \\ h_A &= \left(1 - \frac{2V}{V_m} \right) (1 - n\tau) \tau \\ h_B &= (1 - n\tau) \left(1 - \frac{pCS\tau}{(C+V)^2} \right) \\ &\quad + \frac{mpV\tau^2}{C+V} \left(1 - \frac{2V}{V_0} \right) \end{aligned} \tag{2.5}$$

Equations (2.5) lead to:

$$h_{flip} = \frac{2n - \frac{4}{\tau} + (2 - n\tau) \frac{pCS}{(C+V)^2} - \frac{mpV\tau}{C+V} \left(1 - \frac{2V}{V_0} \right)}{(2 - n\tau) \left(1 - \frac{2V}{V_m} \right)} \tag{2.6}$$

When the above conditions are met, two eigenvalues become $\lambda_1 = -1$ and $\lambda_2 = tr(J) + 1$, The occurrence of Flip bifurcation needs to satisfy $|\lambda_2| \neq 1$, which is

$$\begin{aligned} h_{flip} \left(1 - \frac{2V}{V_m} \right) (1 - n\tau) \tau + (1 - n\tau) \left(1 - \frac{pCS\tau}{(C+V)^2} \right) \\ + \frac{mpV\tau^2}{C+V} \left(1 - \frac{2V}{V_0} \right) \neq \pm 1 \end{aligned} \tag{2.7}$$

When h_{flip} satisfies equation (2.7), let

$$w = S - S_1, \quad z = V - V_1, \quad \tilde{h} = h - h^* \tag{2.8}$$

And we obtain a new map:

$$\begin{pmatrix} w \\ z \\ \tilde{h} \end{pmatrix} \to \begin{pmatrix} a_{11} w + a_{12} z + a_{13} z^2 + O\left(\left(|w| + |z| + \left| \tilde{h} \right| \right)^4 \right) \\ a_{21} w + a_{22} z + a_{23} z^2 + a_{24} wz + a_{25} z^3 + a_{26} wz^2 + a_{27} \tilde{h} \\ + a_{28} \tilde{h} z + a_{29} h z^2 + O\left(\left(|w| + |z| + \left| \tilde{h} \right| \right)^4 \right) \\ \tilde{h} \end{pmatrix} \tag{2.9}$$

in which

$$\begin{aligned} a_{11} &= 1 - n\tau, a_{12} = \frac{\tau m (-2V_1 + V_0)}{V_0}, \\ a_{13} &= -\frac{m\tau}{V_0}, a_{21} = -\frac{\tau p V_1}{C + V_1}, \\ a_{22} &= 1 + \tau \left(h - \frac{2hV_1}{V_m} - \frac{pS_1 C}{(C + V_1)^2} \right), \\ a_{23} &= \left(\frac{CpS_1}{(C + V_1)^3} - \frac{h}{V_m} \right) \tau, \\ a_{24} &= \frac{\tau p V_1}{(C + V_1)^2} - \frac{\tau p}{C + V_1}, \quad a_{25} = -\frac{CpS_1 \tau}{(C + V_1)^4}, \\ a_{26} &= -\frac{\tau p V_1}{2 (C + V_1)^3} + \frac{\tau p}{(C + V_1)^2} \\ a_{27} &= V_1 \tau \left(1 - \frac{V_1}{V_m} \right), \quad a_{28} = \tau \left(1 - \frac{2V_1}{V_m} \right), \\ a_{29} &= \frac{\tau}{V_m} \end{aligned} \tag{2.10}$$

The h values in all equations in (2.10) satisfy $h = h^*$. Apply the following reversible transform to the map (2.9)

$$\begin{pmatrix} w \\ z \end{pmatrix} = \begin{pmatrix} a_{12} & a_{12} \\ -1 - a_{11} & \lambda_2 - a_{11} \end{pmatrix} \begin{pmatrix} \tilde{w} \\ \tilde{z} \end{pmatrix} \tag{2.11}$$

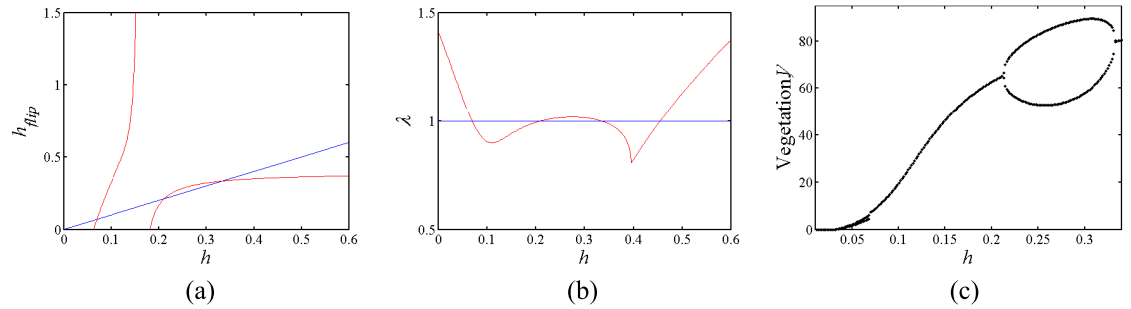

FIGURE 3. Solving the critical point, Bifurcation diagram, Eigenvalue function graph and phase portraits of Flip bifurcation. (a) The red curve is h_{flip} (h) and the blue curve is h; (b) The red curve is λ (h) and the blue curve is λ = 1; (c) Bifurcation diagram with parameters: $m = 0.2$; $n = 0.45$; $\tau = 5$; $p = 0.27$; $k_0 = 0.45$; $V_m = 100\%$; $V_0 = 200\%$; $C = 10\%$.

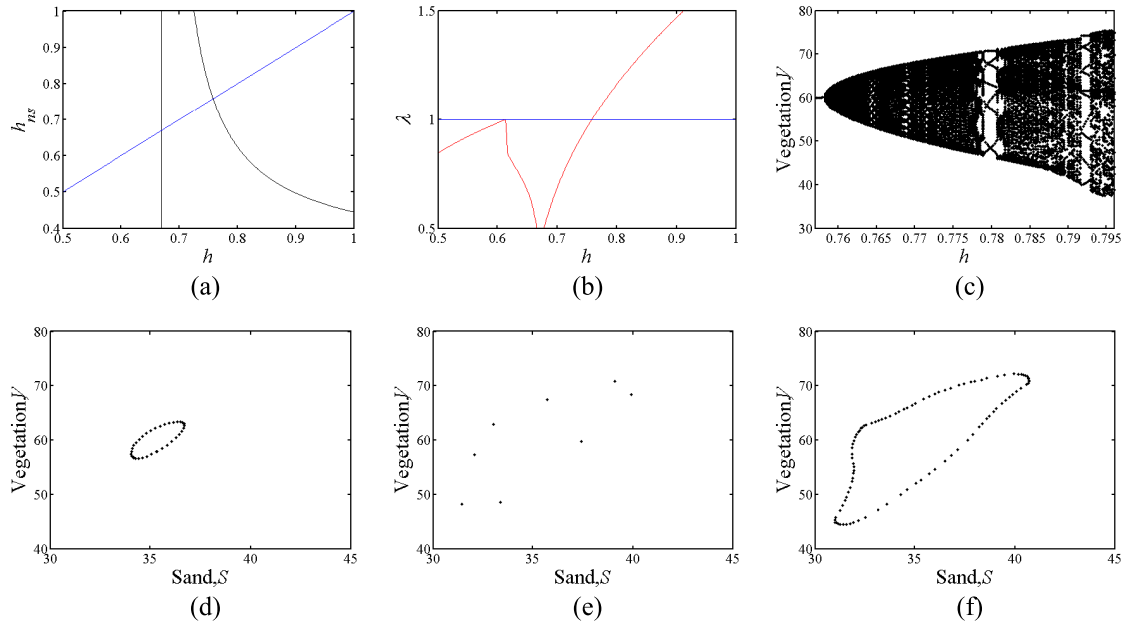

FIGURE 4. Solving the critical point, Bifurcation diagram, Eigenvalue function graph and phase portraits of Neimark-Sacker bifurcation. (a) The black curve is h_{ns} (h) and the blue curve is h; (b) The red curve is λ (h) and the blue curve is λ = 1; (c) Bifurcation diagram with parameters: $m = 0.2$; $n = 0.5$; $\tau = 5$; $p = 0.6$; $k_0 = 9.26$; $V_m = 100\%$; $V_0 = 200\%$; $C = 10\%$; (d–f) Phase portraits with parameter (d) $h = 0.76$; (e) $h = 0.78$; $h = 0.785$.

Then this map becomes

$$\begin{pmatrix}\tilde{w}\\ \tilde{z}\end{pmatrix} \to \begin{pmatrix}-1 & 0\\ 0 & \lambda_2\end{pmatrix}\begin{pmatrix}\tilde{w}\\ \tilde{z}\end{pmatrix} + \frac{1}{a_{12}(1+\lambda_2)} \times \begin{pmatrix}F_1\left(\tilde{w},\tilde{z},\tilde{h}\right)\\ F_2\left(\tilde{w},\tilde{z},\tilde{h}\right)\end{pmatrix} \quad (2.12)$$

which is

$$\begin{aligned} &F_1\left(\tilde{w},\tilde{z},\tilde{h}\right)\\ &= a_{12}^2 a_{24}\left(\tilde{w}+\tilde{z}\right)\left[\left(1+a_{11}\right)\tilde{w}-\left(\lambda_2-a_{11}\right)\tilde{z}\right]\\ &\quad+\left[a_{13}\left(\lambda_2-a_{11}\right)-a_{12}a_{23}\right]\left[\left(1+a_{11}\right)\tilde{w}-\left(\lambda_2-a_{11}\right)\tilde{z}\right]^2\\ &\quad-a_{12}^2 a_{26}\left(\tilde{w}+\tilde{z}\right)\left[\left(1+a_{11}\right)\tilde{w}-\left(\lambda_2-a_{11}\right)\tilde{z}\right]^2\\ &\quad+a_{12}a_{25}\left[\left(1+a_{11}\right)\tilde{w}-\left(\lambda_2-a_{11}\right)\tilde{z}\right]^3-a_{12}a_{27}\tilde{h}\\ &\quad+a_{12}a_{28}\tilde{h}\left[\left(1+a_{11}\right)\tilde{w}-\left(\lambda_2-a_{11}\right)\tilde{z}\right]\\ &\quad-a_{12}a_{29}\tilde{h}\left[\left(1+a_{11}\right)\tilde{w}-\left(\lambda_2-a_{11}\right)\tilde{z}\right]^2 \end{aligned} \quad (2.13)$$

$$\begin{aligned} &F_2\left(\tilde{w},\tilde{z},\tilde{h}\right)\\ &= -a_{12}^2 a_{24}\left(\tilde{w}+\tilde{z}\right)\left[\left(1+a_{11}\right)\tilde{w}-\left(\lambda_2-a_{11}\right)\tilde{z}\right]\\ &\quad+\left[a_{13}\left(1+a_{11}\right)+a_{12}a_{23}\right]\left[\left(1+a_{11}\right)\tilde{w}-\left(\lambda_2-a_{11}\right)\tilde{z}\right]^2\\ &\quad+a_{12}^2 a_{26}\left(\tilde{w}+\tilde{z}\right)\left[\left(1+a_{11}\right)\tilde{w}-\left(\lambda_2-a_{11}\right)\tilde{z}\right]^2\\ &\quad-a_{12}a_{25}\left[\left(1+a_{11}\right)\tilde{w}-\left(\lambda_2-a_{11}\right)\tilde{z}\right]^3+a_{12}a_{27}\tilde{h}\\ &\quad-a_{12}a_{28}\tilde{h}\left[\left(1+a_{11}\right)\tilde{w}-\left(\lambda_2-a_{11}\right)\tilde{z}\right]\\ &\quad+a_{12}a_{29}\tilde{h}\left[\left(1+a_{11}\right)\tilde{w}-\left(\lambda_2-a_{11}\right)\tilde{z}\right]^2 \end{aligned} \quad (2.14)$$

Use center manifold theorem, There is a central manifold $W^c(0,0,0)$ at the fixed point (0, 0, 0), which can be approximated by the following formula.

$$W^c(0,0,0)=\left\{\left(\tilde{w},\tilde{z},\tilde{h}\right)\in R^3 \mid \tilde{z}=T^*\left(\tilde{w},\tilde{h}\right), T^*(0,0)=0, DT^*(0,0)=0\right\} \quad (2.15)$$

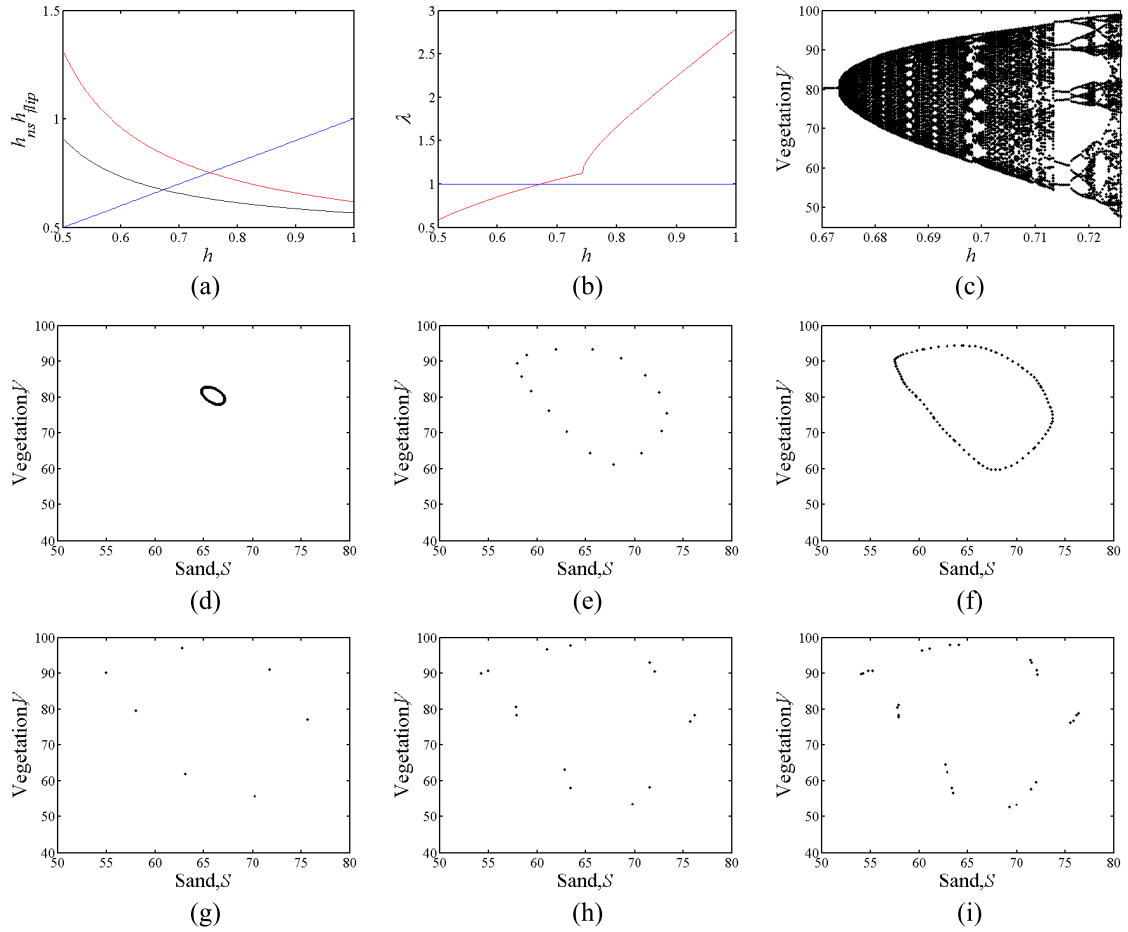

FIGURE 5. Solving the critical point, Bifurcation diagram, Eigenvalue function graph and phase portraits of Neimark-Sacker bifurcation. (a) The red, black, blue curve is h_{flip} (h), h_{ns} (h) and h, respectively; (b) The red curve is λ (h) and the blue curve is $\lambda = 1$; (c) Bifurcation diagram with parameters: $m = 0.2cm \cdot d^{-1}$; $n = 0.35$; $\tau = 5$; $p = 0.18$; $k_0 = 13.47$; $V_m = 100\%$; $V_0 = 200\%$; $C = 10\%$; (d–i) Phase portraits with parameter (d) $h = 0.6735$; (e) $h = 0.6986$; (f) $h = 0.702$; (g) $h = 0.7134$; (h) $h = 0.718$; (i) $h = 0.7193$.

where $T^*\left(\tilde{w}, \tilde{h}\right)$ is assumed to be

$$T^*\left(\tilde{w}, \tilde{h}\right) = e_0\tilde{h} + e_1\tilde{w}^2 + e_2\tilde{w}\tilde{h} + e_3\tilde{h}^2 + O\left(\left(|\tilde{w}| + \left|\tilde{h}\right|\right)^3\right) \tag{2.16}$$

According to $\tilde{z} = T^*\left(\tilde{w}, \tilde{h}\right)$, there is

$$\begin{aligned} & e_0\tilde{h} + e_1\left(-\tilde{w} + \frac{F_1\left(\tilde{w}, T^*\left(\tilde{w}, \tilde{h}\right), \tilde{h}\right)}{a_{12}\left(1+\lambda_2\right)}\right)^2 \\ & + e_2\tilde{h}\left(-\tilde{w} + \frac{F_1\left(\tilde{w}, T^*\left(\tilde{w}, \tilde{h}\right), \tilde{h}\right)}{a_{12}\left(1+\lambda_2\right)}\right) + e_3\tilde{h}^2 \\ & - \lambda_2\left(e_0\tilde{h} + e_1\tilde{w}^2 + e_2\tilde{w}\tilde{h} + e_3\tilde{h}^2\right) - \frac{F_2\left(\tilde{w}, T^*\left(\tilde{w}, \tilde{h}\right), \tilde{h}\right)}{a_{12}\left(1+\lambda_2\right)} \\ & = O\left(\left(|\tilde{w}| + \left|\tilde{h}\right|\right)^3\right) \end{aligned} \tag{2.17}$$

Using the balance of the left and right sides of equation (2.17), the values of the coefficients e_0, e_1, e_2 and e_3 can be determined.

$$\begin{aligned} e_0 &= \frac{a_{27}}{1-\lambda^2} \\ e_1 &= \frac{\left(a_{11}+1\right)^3 a_{13} + \left(a_{11}+1\right)^2 a_{12}a_{23} - \left(a_{11}+1\right) a_{12}^2 a_{24}}{a_{12}\left(1-\lambda_2^2\right)} \\ e_2 &= \frac{a_{28}\left(1+a_{11}\right)}{\left(1+\lambda_2\right)^2} \\ e_3 &= 0 \end{aligned} \tag{2.18}$$

Correspondingly, considering the mapping (2.12) to limit the dynamic part of the center manifold $W^c(0, 0, 0)$, a one-dimensional mapping can be obtained.

$$\begin{aligned} F : \tilde{w} \to & -\tilde{w} + \mu_1\tilde{w}^2 + \mu_2\tilde{w}\tilde{h} + \mu_3\tilde{w}^2\tilde{h} + \mu_4\tilde{w}\tilde{h}^2 + \mu_5\tilde{w}^3 \\ & + O\left(\left(|\tilde{w}| + \left|\tilde{h}\right|\right)^4\right) \end{aligned} \tag{2.19}$$

The coefficients in this map are expressed as follows,

$$\begin{aligned} \mu_1 = \frac{1}{a_{12}\left(1+\lambda_2\right)} & \left(\left(a_{13}\left(\lambda_2 - a_{11}\right) - a_{12}a_{23}\right)\left(1+a_{11}\right)^2 \right. \\ & \left. + a_{12}^2 a_{24}\left(1+a_{11}\right)\right) \end{aligned}$$

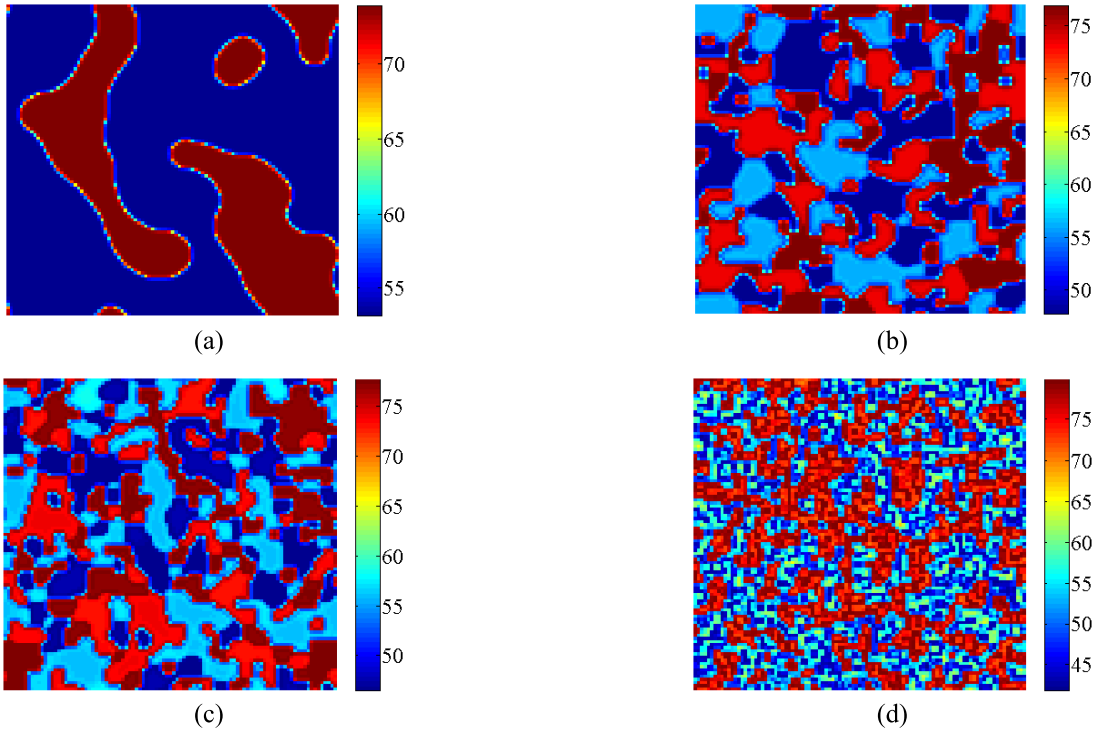

FIGURE 6. Patterns induced by Flip bifurcation. Parameters: $m = 0.2$; $n = 0.07$; $\tau = 2$; $p = 0.45$; $k_0 = 4.36$; $V_m = 100\%$; $V_0 = 200\%$; $C = 10\%$; $d =$; $d_1 = 0.01$; $d_2 = 0.1$; $a_1 = 0$; $a_2 = 0$; (a) $h = 3.235$; (b) $h = 3.28$; (c) $h = 3.293$; (d) $h = 3.327$; $t = 2000$.

$$
\begin{aligned}
\mu_2 &= \frac{a_{28}\,(1+a_{11})}{1+\lambda_2}\\
\mu_3 &= \frac{1}{a_{12}\,(1+\lambda_2)}\,(2\,(a_{13}\,(\lambda_2-a_{11})-a_{12}a_{23})\\
&\quad\times\left(e_0e_1\,(\lambda_2-a_{11})^2-e_2\,(1+a_{11})\,(\lambda_2-a_{11})\right)\\
&\quad+a_{12}^2a_{24}\,(e_2\,(1-\lambda_2+2a_{11})-2e_0e_1\,(\lambda_2-a_{11}))\\
&\quad-a_{12}^2a_{26}e_0\,(1+a_{11})\,(1+3a_{11}-2\lambda_2)-3a_{12}a_{25}e_0\\
&\quad\times(1+a_{11})^2\,(\lambda_2-a_{11})-a_{12}a_{28}e_1\,(\lambda_2-a_{11})\\
&\quad-a_{12}a_{29}\,(1+a_{11})^2\Big)\\
\mu_4 &= \frac{1}{a_{12}\,(1+\lambda_2)}\Big(2e_0e_2\,(\lambda_2-a_{11})\,((a_{13}\,(\lambda_2-a_{11})\\
&\quad-a_{12}a_{23})\,(\lambda_2-a_{11})-a_{12}^2a_{24}\Big)-a_{12}e_0^2\,(\lambda_2-a_{11})^2\\
&\quad\times(a_{12}a_{26}+3a_{25}\,(1+a_{11}))-a_{12}a_{28}e_2\,(\lambda_2-a_{11})\\
&\quad-2a_{12}a_{29}e_0\,(1+a_{11})\,(\lambda_2-a_{11}))\\
\mu_5 &= 2e_1\,(a_{13}\,(\lambda_2-a_{11})-a_{12}a_{23})\,(1+a_{11})\,(\lambda_2-a_{11})\\
&\quad+a_{12}^2a_{24}e_1\,(1-\lambda_2+2a_{11})-a_{12}^2a_{26}\,(1+a_{11})^2\\
&\quad+a_{12}a_{25}\,(1+a_{11})^3
\end{aligned}
\tag{2.20}
$$

The occurrence of the period-doubling bifurcation of the map (2.19) requires that the two judgment amounts η_1 and η_2 are not zero, and the two determination amounts can be obtained by the following formula.

$$
\eta_1 = \left(\frac{\partial^2 F}{\partial\tilde{w}\partial\tilde{h}}+\frac{1}{2}\frac{\partial F}{\partial\tilde{h}}\frac{\partial^2 F}{\partial^2\tilde{w}}\right),\quad \left(\tilde{w}=0,\tilde{h}=0\right)
$$

$$
\eta_2 = \left(\frac{1}{6}\frac{\partial^3 F}{\partial^3\tilde{w}}+\left(\frac{1}{2}\frac{\partial^2 F}{\partial^2\tilde{w}}\right)^2\right),\quad \left(\tilde{w}=0,\tilde{h}=0\right) \tag{2.21}
$$

Then,

$$
\eta_1 = \mu_2,\quad \eta_2 = \mu_5+\mu_1^2 \tag{2.22}
$$

Summarizing the above calculations, the conditions for the occurrence of period-doubling bifurcation in discrete systems can be described as:

If equations (2.6) and (2.7) are true and the conditions $\mu_2 \neq 0$ and $\mu_5 \neq -\mu_1^2$ are satisfied, the Flip bifurcation is experienced at the fixed point (S_1, V_1). Moreover, if $\eta_2 > 0$, the period -2 points branched from (S_1, V_1) are stable; if $\eta_2 < 0$, the period -2 points of the splitting are unstable.

As long as we solve for $h_{flip} = h$, we can get the critical point h_0 of the system. We can clearly see that the two curves on the coordinate axis have intersections, so we get a stable critical point $h = h_0 = 3.1478$ in Figure 2a. Figure 2b shows the curve of the eigenvalue λ with respect to the parameter h. Where $h = h_0 = 3.1478d^{-1}$, $\lambda = 1$. Figure 2c shows variations of V versus the parameter h when the parameter values satisfy the flip bifurcation conditions. When the eigenvalue λ is less than 1, the system is stable, when it is greater than 1, the system starts to occur bifurcation. So in combination with Figure 2a and Figure 2b we can know when $h < 3.1478d^{-1}$, the fixed point is asymptotically stable. When $h = 3.1478d^{-1}$, the system starts to bifurcate around a fixed point as shown in Figure 1c. With the increase of h, the stable states of the system go

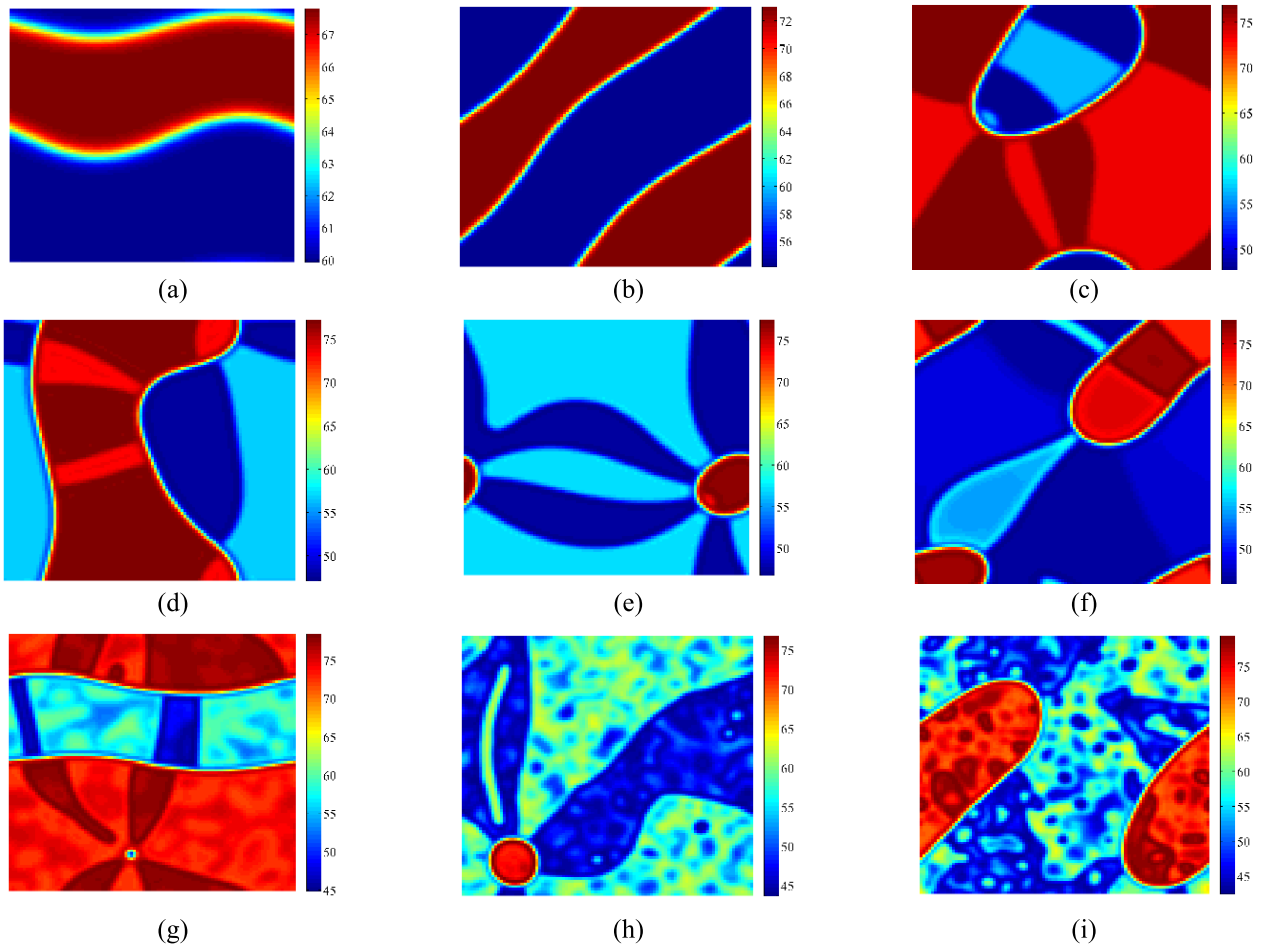

FIGURE 7. Patterns induced by Flip bifurcation. Parameters: $m = 0.2$; $n = 0.07$; $\tau = 2$; $p = 0.45$; $k_0 = 4.36$; $V_m = 100\%$; $V_0 = 200\%$; $C = 10\%$; $d = 2$; $d_1 = 0.02$; $d_2 = 0.4$; $a_1 = 0.01$; $a_2 = 0.02$; (a) $h = 3.16$; (b) $h = 3.22$; (c) $h = 3.28$; (d) $h = 3.285$; (e) $h = 3.289$; (f) $h = 3.297$; (g) $h = 3.305$; (h) $h = 3.313$; (i) $h = 3.319$; $t = 2000$.

through (not only these states) period-2 ($h = 3.2d^{-1}$ as shown in Figure 2d), period-4 ($h = 3.28d^{-1}$ as shown in Figure 2e), period-8 ($h = 3.293d^{-1}$ as shown in Figure 2f) and then complex periodic oscillations ($h = 3.327d^{-1}$as shown in Figure 2g).

At the same time, we found an interesting thing in the process of simulating Flip bifurcation. In Figure 3a, We can get 3 critical point solutions: $h_1 = 0.0694d^{-1}$, $h_2 = 0.2119d^{-1}$, $h_3 = 0.3339d^{-1}$. From Figure 3b we can see that the system occurs bifurcations in the ranges $h < 0.0694d^{-1}$ and $0.2119d^{-1} < h < 0.3339d^{-1}$. Combined with Figure 3a and Figure 3b, we get the corresponding bifurcation diagram in Figure 3c. The system bifurcates at the critical point $h = 0.2119d^{-1}$, after which it does not perform double-cycle divergence like the conventional Flip bifurcation, but keeps the 2-cycle mode converging to the next critical point $h = 0.3339d^{-1}$.

C. NEIMARK-SACKER BIFURCATION ANALYSIS

The theoretical part of the Neimark-Sacker bifurcation analysis is detailed in [34]. The solution process is the same as the previous section. So we get

$$h_{ns} = \frac{n + \frac{pSC(1-n\tau)}{(C+V)^2} + \frac{mp\tau V(2V-V_0)}{V_0(C+V)}}{(1-n\tau)\left(1-\frac{2V}{V_m}\right)} \tag{2.23}$$

Similarly, we can get the curve of the solution of the critical point under Neimark-Sacker bifurcation condition by Equation (2.23). We can see from Figure 4a that the critical point is at $h = 0.7582d^{-1}$. Then we know that the Neimark-Sacker bifurcation occurs when the range $h > 0.7582d^{-1}$ in Figure 4b. Figure 4c shows the variations of V versus parameter h when the parameter values satisfy the Neimark-Sacker bifurcation condition. When $h < 0.7582d^{-1}$, the fixed point is asymptotically stable. When $h = 0.7582d^{-1}$, the system starts to bifurcate around a fixed point. As the value of h increases, the stable states of the system in the phase plane (V, S) experience several stages, such as invariant circle ($h = 0.76d^{-1}$ as shown in Figure 4d), period-8 ($h = 0.78d^{-1}$ as shown in Figure 4e), and then invariant circle again ($h = 0.785d^{-1}$ as shown in Figure 4f). Then the stable states of the system may go through several multi-period and invariant circle stages.

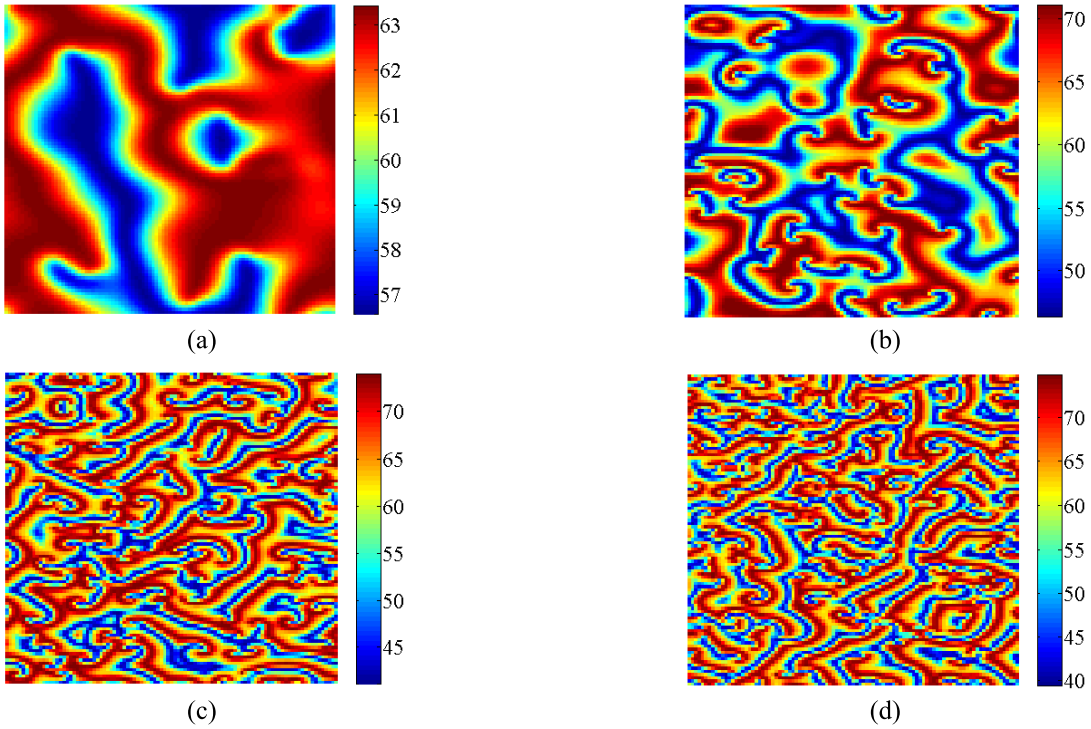

FIGURE 8. Patterns induced by Neimark-Sacker bifurcation. Parameters: $m = 0.2$; $n = 0.5$; $\tau = 5$; $p = 0.6$; $k_0 = 9.26$; $V_m = 100\%$; $V_0 = 200\%$; $C = 10\%$; $d = 2m$; $d_1 = 0.01$; $d_2 = 0.01$; $a_1 = 0.015$; $a_2 = 0.012$; (a) $h = 0.76$; (b) $h = 0.78$; (c) $h = 0.7921$; (d) $h = 0.795$; $t = 2000$.

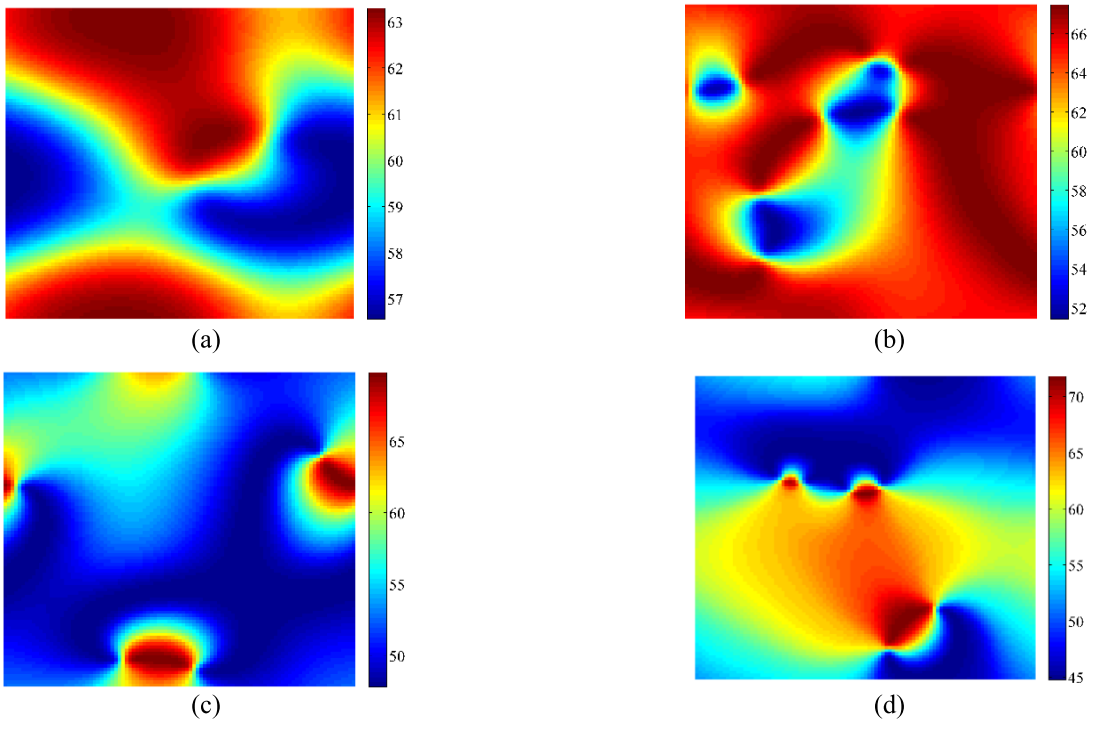

FIGURE 9. Patterns induced by Neimark-Sacker bifurcation. Parameters: $m = 0.2$; $n = 0.5$; $\tau = 5$; $p = 0.6$; $k_0 = 9.26$; $V_m = 100\%$; $V_0 = 200\%$; $C = 10\%$; $d = 2$; $d_1 = 0.1$; $d_2 = 0.01$; $a_1 = 0.01$; $a_2 = 0.01$; (a) $h = 0.76$; (b) $h = 0.768$; (c) $h = 0.76$; (d) $h = 0.784$; $t = 2000$.

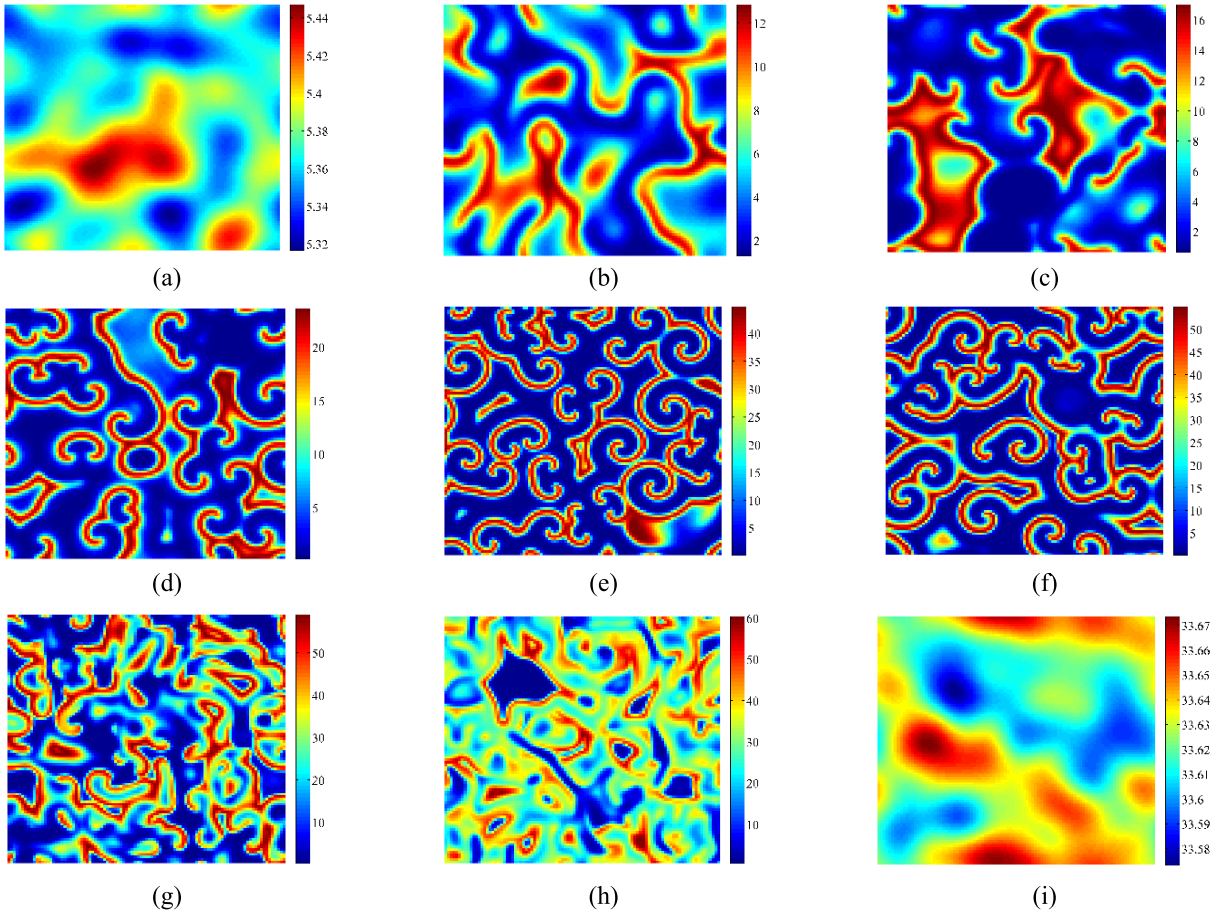

FIGURE 10. Patterns induced by Neimark-Sacker bifurcation. Parameters: $m = 0.2$; $n = 0.21$; $\tau = 0.5$; $p = 0.9$; $k_0 = 1.5$; $V_m = 100\%$; $V_0 = 200\%$; $C = 10\%$; $d = 2$; $d_1 = 0.1$; $d_2 = 0.1$; $a_1 = 0$; $a_2 = 0$; (a) $h = 0.75$; (b) $h = 0.76$; (c) $h = 0.77$; (d) $h = 0.79$; (e) $h = 0.88$; (f) $h = 0.97$; (g) $h = 1.01$; (h) $h = 1.03$; (i) $h = 1.05$; t = 2000.

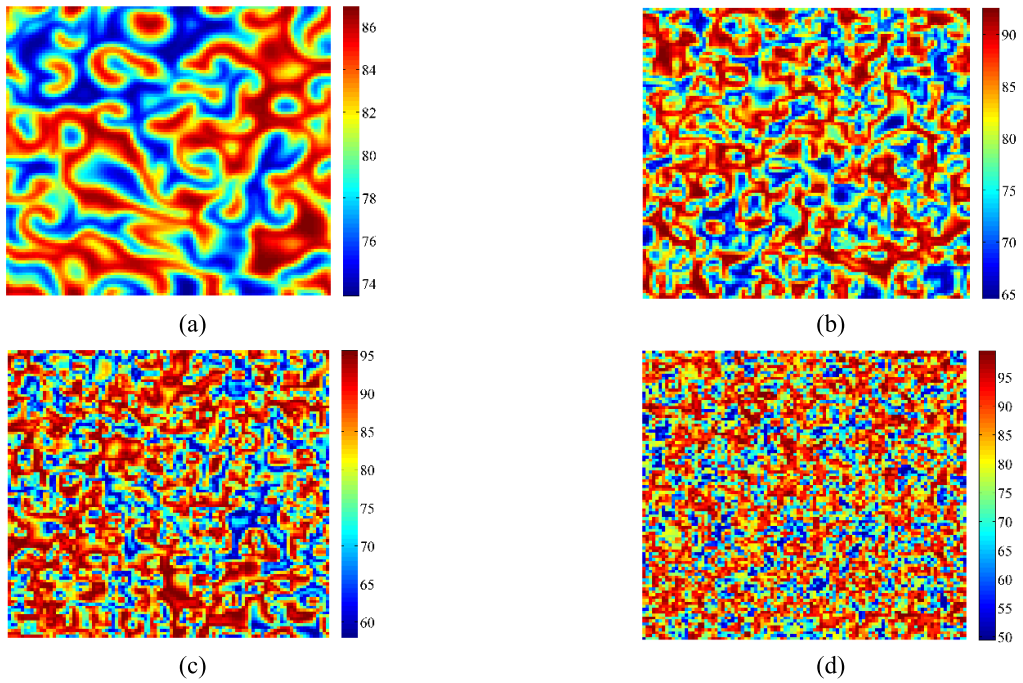

FIGURE 11. Patterns induced by Neimark-Sacker-Flip bifurcation. Parameters: $m = 0.2$; $n = 0.35$; $\tau = 5$; $p = 0.18$; $k_0 = 13.47$; $V_m = 100\%$; $V_0 = 200\%$; $C = 10\%$; $d = 2$; $d_1 = 0.01$; $d_2 = 0.01$; $a_1 = 0$; $a_2 = 0$; (a) $h = 0.675$; (b) $h = 0.69$; (c) $h = 0.705$; (d) $h = 0.725$; $t = 2000$.

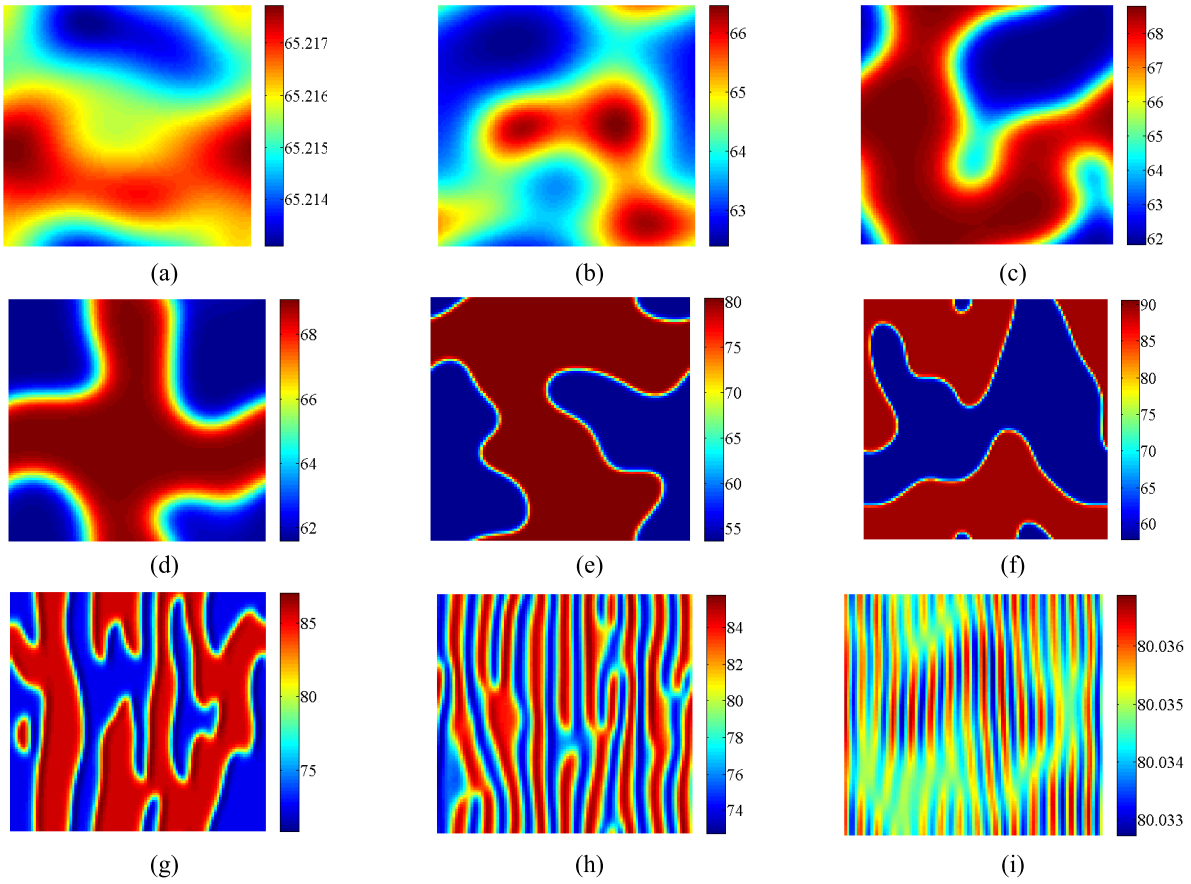

FIGURE 12. Patterns induced by Turing-Flip bifurcation. Parameters: $m = 0.2$; $n = 0.45$; $\tau = 5$; $p = 0.27$; $k_0 = 0.45$; $V_m = 100\%$; $V_0 = 200\%$; $C = 10\%$; $d = 2$; $d_1 = 0.009$; $d_2 = 0.019$; $a_1 = 0.009$; $a_2 = 0.05$; (a) $h = 0.2119$; (b) $h = 0.2132$; (c) $h = 0.2135$; (d) $h = 0.2137$; (e) $h = 0.24$; (f) $h = 0.3$; (g) $h = 0.33$; (h) $h = 0.3322$; (i) $h = 0.3355$; $t = 10000$.

D. NEIMARK-SACKER-FLIP BIFURCATION ANALYSIS

In this section simulations will be carried out when both Neimark-Sakcer and Flip bifurcation occur. We start by adjusting the critical value of both. In Figure 5a, the intersection of the black and blue curves is the critical point of Neimark-Sacker, and the intersection of the red and blue curves is the critical point of Flip. They both have the same eigenvalue λ, and the curve of the eigenvalue λ as a function of h is shown in Figure 5b. Figure 5b does not show the critical point of Flip in Figure 5a, indicating that the critical point in Figure 5a is a non-existent solution, thus there are has no stable states in Flip bifurcation. To get Flip and Neimark-Sacker bifurcation at the same time, the interval between the two must have an intersection. Combined with Figure 5a and Figure 5b, we can see that when $h > 0.6733d^{-1}$, the coupled bifurcation occurs. Figure 5c shows the variations of V versus parameter h when the parameter values satisfy the coupled bifurcation condition. In the first half of the bifurcation diagram, it is similar to the Neimark-Sacker bifurcation, and in the latter half, the same period bifurcation as the Flip bifurcation occurs.

III. VEGETATION PATTERN SELF-ORGANIZATION FORMED BY BIFURCATIONS

In order to investigate the formation of self-organized patterns under the above bifurcation conditions, simulations will be carried out on 100×100 lattices with periodic boundary conditions. Initial conditions are set as fixed points with heterogeneous random disturbance (1%). Given the parameter values under each bifurcation condition, the formation of patterns can be obtained after $t = 2000$ or longer. Patterns will be shown only in terms of variable V, as the patterns of variable S are similar.

The color scale in all the following figures are automatically selected by the software MATLAB 7.12.0 (2011a) command "pcolor" according to the minimum and the maximum values of vegetation cover at each time. Precisely, the blue area represents low vegetation coverage, while the red area represents high vegetation coverage. Sometime, the minimum value of vegetation coverage reaches zero, which means vegetation dies out in the vegetation-sand system and only bare sand can be seen.

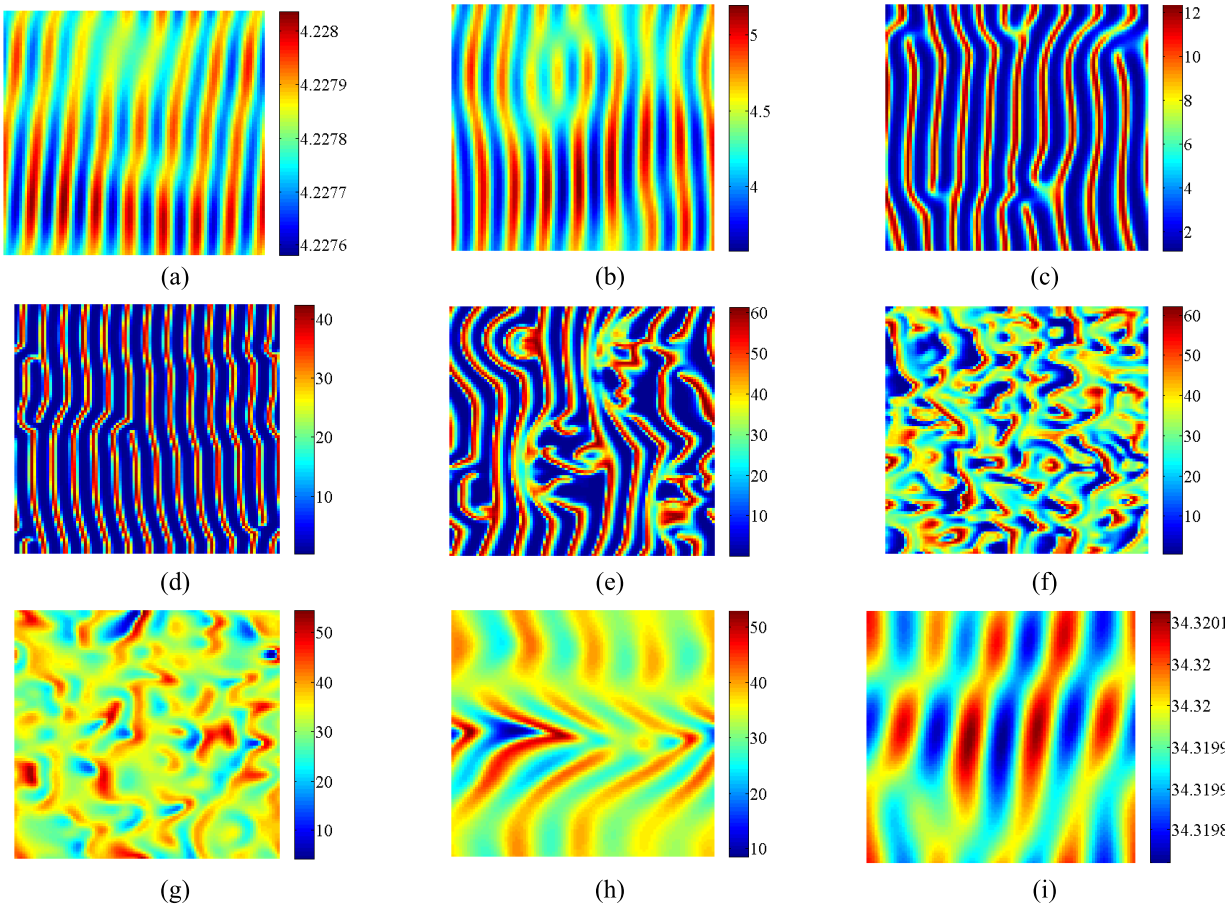

FIGURE 13. Patterns induced by Turing-Neimark-Sacker bifurcation. Parameters: $m = 0.2$; $n = 0.21$; $\tau = 0.5$; $p = 0.9$; $k_0 = 1.5$; $V_m = 100\%$; $V_0 = 200\%$; $C = 10\%$; $d = 2$; $d_1 = 0.07$; $d_2 = 0.07$; $a_1 = 0.2$; $a_2 = 0.08$; (a) $h = 0.7321$; (b) $h = 0.734$; (c) $h = 0.742$; (d) $h = 0.85$; (e) $h = 1.01$; (f) $h = 1.03$; (g) $h = 1.05$; (h) $h = 1.054$; (i) $h = 1.058$; $t = 10000$.

A. FLIP BIFURCATION ON VEGETATION PATTERN SELF-ORGANIZATION

Figure 6 shows the patterns induced by Flip bifurcation. We can see that patterns are formed through self-organization of variable V. With the increase of h, the patterns is getting broken.

When we changed a set of parameters, the irregular shape is showed in the pattern while maintaining the fold period characteristics of the Flip bifurcation in Figure 7(a-i).

B. NEIMARK-SACKER BIFURCATION ON VEGETATION PATTERN SELF-ORGANIZATION

Figure 8 shows the patterns induced by Neimark-Sacker bifurcation, and $h_0 = 0.7582d^{-1}$ satisfy the Neimark-Sacker bifurcation conditions. Patterns are formed through self-organization of variable V. With the increase of h, The pattern becomes thinner.

Also, we changed a set of parameters and found that the pattern has a blocky highlight area. With the increase of h, The red area, that is, the larger value, is gradually reduced in Figure 9.

Figure 10 shows another series of vegetation patterns with the increase of h. When $h > h_1 = 0.7466d^{-1}$, Neimark-Sacker bifurcation occurs and $h > h_2 = 1.0508d^{-1}$, the system returns to stability. Figure 10d-f show the curled striped vegetation patterns. And the curled striped vegetation patterns changed as shown in Figure 10g-i.

C. NEIMARK-SACKER-FLIP BIFURCATION ON VEGETATION PATTERN SELF-ORGANIZATION

Figure 11 shows the patterns induced by Neimark-Sacker-Flip bifurcation, and $h_0 = 0.6733d^{-1}$ satisfy the Neimark-Sacker-Flip bifurcation conditions. We can see that patterns are formed through self-organization of variable V. With the increase of h, The pattern becomes more complex and denser.

D. COUPLED EFFECTS OF TURING AND FLIP BIFURCATIONS ON VEGETATION PATTERN SELF-ORGANIZATION

Firstly, vegetation patterns induced by Turing-flip bifurcation are shown in Figure 12. Figure 12a, b show the light and dark spots, And Figure 12c is the transition state, Figure 12d is the prototype of the patterns induced by Flip

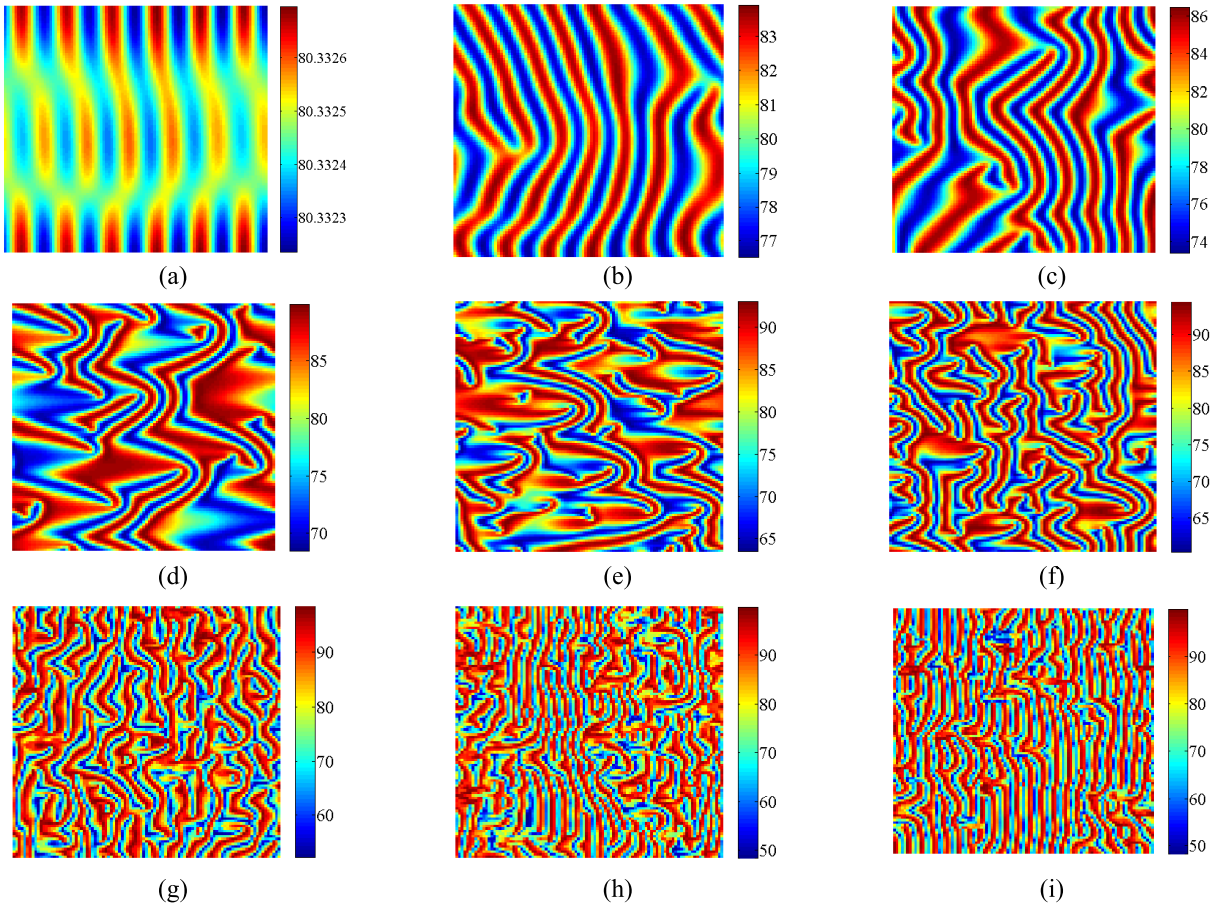

FIGURE 14. Patterns induced by Turing-Neimark-Sacker-Flip bifurcation. Parameters: $m = 0.2$; $n = 0.35$; $\tau = 5$; $p = 0.18$; $k_0 = 13.47$; $V_m = 100\%$; $V_0 = 200\%$; $C = 10\%$; $d = 2$; $d_1 = 0.01$; $d_2 = 0.015$; $a_1 = 0.085$; $a_2 = 0.01$; (a) $h = 0.6682$; (b) $h = 0.06698$; (c) $h = 0.673$; (d) $h = 0.681$; (e) $h = 0.692$; (f) $h = 0.7$; (g) $h = 0.722$; (h) $h = 0.73$; (i) $h = 0.7335$; $t = 10000$.

bifurcation, and Figure 12e, f is typical patterns of Flip bifurcation. The coupling effect of Flip and Turing can be clearly seen in Figure 12g, and Figure 12h, i is typical Turing pattern. Combining all nine images to see the coupling result of Turing and Flip bifurcation, the effect of Flip is strong first and then weak, while Turing is just the opposite. In other words, during the formation of the pattern induced by Flip bifurcation, Turing showed effect in the second half.

E. COUPLED EFFECTS OF TURING AND NEIMARK-SACKER BIFURCATIONS ON VEGETATION PATTERN SELF-ORGANIZATION

Figure 13 shows the vegetation patterns induced by Turing-Neimark-Sacker bifurcation. Figure 13a is the corresponding pattern at the beginning of the bifurcation. It can be seen that the effect of Turing is very strong, and Figure 13b-d is still dominated by Turing. In Figure 13e we can clearly see that the effect of Neimark-Sacker gradually emerges, occupying the pattern with Turing. Figure 13f, g shows the Neimark-Sacker type pattern, Figure 13h, i is the corresponding pattern before the system returns to stability, in Figure 13i, t the pattern is a light-dark, speckled band-like composition. Combining all nine images to see the coupling result of Turing and Neimark-Sacker bifurcation, the effect of Turing is strong first and then weak, while Neimark-Sacker is the opposite, and the effect of Turing occupies a larger interval. In other words, in the range of $0.7321d^{-1} < h < 1.01d^{-1}$, Turing dominates, and in the range of $1.01d^{-1} < h < 1.058d^{-1}$, the effect of Neimark-Sacker is more obvious.

F. COUPLED EFFECTS OF TURING, NEIMARK-SACKER AND FLIP BIFURCATIONS ON VEGETATION PATTERN SELF-ORGANIZATION

Figure 14 shows the vegetation patterns induced by Turing-Neimark-Sacker-Flip bifurcation. From the figure, the coupling of the three is more complicated than the coupling of the two. As shown in Figure 14a, at the beginning of the pattern, the pattern is a light-dark, speckled band-like composition. Combined with all the images, the effect of Turing seems to always exist, but it is weak in Figure 14d, e. The effect of Neimark-Sacker also plays a role in the whole process. Throughout the process, the role of Flip seems to be making the pattern more and more complicated.

IV. DISCUSSION

From the bifurcation diagram, particularly in Figure 5c, the system first occurs with Neimark-Sacker bifurcation and then mutates into Flip bifurcation. In Figure 5b, the eigenvalue λ is always greater than 1 when $h > 0.6733d^{-1}$, so the Flip bifurcation is generated as the Neimark-Sacker bifurcation occurs in the system. But there exist an h that make the eigenvalue $\lambda = 1$ in Figure 5a. Therefore, the appearance of Flip bifurcation in Neimark-Sacker bifurcation is likely to be caused by this factor. From the simulated patterns, In Figure 5c, we implement the coupling of the Neimark-Sacker-Flip bifurcation, and in Figure 14 we find the coupling pattern of the three after joining Turing. Although at present definitions of the three bifurcations conflict with each other, these simulation results reveal that different bifurcations can be coupled with each other.

In fact, studies on the compatibility of multi-bifurcations have great ecological significance. In the real world, vegetation bands are not perfectly straight. There have been several explanations on this issue. Some researchers think that this may be due to the stochastic micro-topography. There is another interpretation in [10], that the self-organization process takes a very long time (about 10,000 days). Before the regular bands are formed, the values of some parameters may change such as a_1 and a_2, as the speed and the direction of prevailing wind are changing all the time. In this paper, we propose another possible explanation. The coupled effects of Neimark-Sacker, Flip and Turing bifurcations make vegetation patterns more irregular and similar to real vegetation patterns in nature.

DATA AVAILABILITY

Codes that related to all simulations can be available on request. (china907a@163.com)

ACKNOWLEDGMENT

The authors would like to thank L. Wang for his help in writing.

REFERENCES

[1] J. A. S. Kelso, *Dynamic Patterns: The Self-Organization of Brain and Behavior*. Cambridge, MA, USA: MIT Press, 1995.

[2] H. Meinhardt and A. Gierer, "Pattern formation by local self-activation and lateral inhibition," *BioEssays*, vol. 22, no. 8, pp. 753–760, 2000.

[3] P. C. M. Molenaar, "Dynamic models of biological pattern formation have surprising implications for understanding the epigenetics of development," *Res. Hum.*, vol. 11, no. 1, pp. 50–62, Feb. 2014.

[4] R. Eftimie, G. D. Vries, M. A. Lewis, and F. Lutscher, "Modeling group formation and activity patterns in self-organizing collectives of individuals," *Bull. Math. Biol.*, vol. 69, no. 5, p. 1537, Feb. 2007.

[5] P. Ball, N.R. Borley, *The Self-Made Tapestry: Pattern Formation in Nature*, vol. 198. Oxford, U.K.: Oxford Univ. Press, Apr. 2000.

[6] E. Bonabeau, G. Theraulaz, and J. L. Deneubourg, "Mathematical model of self-organizing hierarchies in animal societies," *Bull. Math. Biol.*, vol. 58, no. 4, pp. 661–717, Jul. 1996.

[7] G. F. Oster and J. D. Murray, "Pattern formation models and developmental constraints," *J. Exp. Zool.*, vol. 251, no. 2, pp. 186–202, Aug. 1989.

[8] P. K. Maini, D. L. Benson, and J. A. Sherratt, "Pattern formation in reaction-diffusion models with spatially inhomogeneous diffusion coefficients," *IMA J. Math. Appl. Med. Biol.*, vol. 9, pp. 197–213, Sep. 1992.

[9] D. Araújo, K. Davids, and R. Hristovski, "The ecological dynamics of decision making in sport," *Psychol. Sport Exerc.*, vol. 7, no. 6, pp. 653–676, Nov. 2006.

[10] F. F. Zhang, H. Y. Zhang, M. R. Evans, and T. S. Huang, "Vegetation patterns generated by a wind driven sand-vegetation system in arid and semi-arid areas," *Ecological Complex.*, vol. 31, pp. 21–33, Sep. 2017.

[11] G. S. Okin, B. Murray, and W. H. Schlesinger, "Degradation of sandy arid shrubland environments: Observations, process modelling, and management implications," *J. Arid Environ.*, vol. 47, no. 2, pp. 123–144, Feb. 2001.

[12] D. J. Eldridge and J. F. Leys, "Exploring some relationships between biological soil crusts, soil aggregation and wind erosion," *J. Arid Environ.*, vol. 53, no. 4, pp. 457–466, Apr. 2003.

[13] Y. C. Yan, X. L. Xu, X. P. Xin, G. X. Yang, X. Wang, R. R. Yan, and B. R. Chen, "Effect of vegetation coverage on aeolian dust accumulation in a semiarid steppe of northern China," *Catena*, vol. 87, no. 3, pp. 351–356, Dec. 2011.

[14] H. L. Zhao, R. L. Zhou, and S. Drake, "Effects of aeolian deposition on soil properties and crop growth in sandy soils of northern China," *Geoderma*, vol. 142, nos. 3–4, pp. 342–348, Dec. 2007.

[15] F. F. Zhang, H. Y. Zhang, and T. S. Huang, "Dynamics on the interaction between vegetation growth and Aeolian dust deposition," *Adv. Mater. Res.*, vols. 356–360, pp. 2430–2433, Oct. 2012.

[16] F. Zhang, H. Zhang, T. Huang, T. Meng, and S. Ma, "Coupled effects of turing and neimark-sacker bifurcations on vegetation pattern self-organization in a discrete vegetation-sand model," *Entropy*, vol. 19, no. 9, pp. 1–22, Sep. 2017.

[17] J. A. Sherratt, "History-dependent patterns of whole ecosystems," *Ecological Complex.*, vol. 14, no. 6, pp. 8–20, Jun. 2013.

[18] T. Huang, H. Zhang, H. Yang, N. Wang, and F. Zhang, "Complex patterns in a space- and time-discrete predator-prey model with Beddington-De Angelis functional response," *Commun. Nonlinear Sci. Numer. Simul.*, vol. 43, pp. 182–199, Feb. 2017.

[19] Y. A. Logvin and T. Ackemann, "Interaction between HOPF and static instabilities in a pattern-forming optical system," *Phys. Rev. E, Stat. Phys. Plasmas Fluids Relat. Interdiscip. Top.*, vol. 58, no. 2, p. 1654, Aug. 1998.

[20] R. Wu, Y. Shao, Y. Zhou, and L. Chen, "Turing and HOPF bifurcation of Gierer-Meinhardt activator-substrate model," *Electron. J. Differ. Equ.*, vol. 2017, no. 173, pp. 1–19, 2017.

[21] Y. Song, T. Zhang, and M. O. Tadé, "Stability switches, HOPF bifurcations, and spatio-temporal patterns in a delayed neural model with bidirectional coupling," *J. Nonlinear Sci.*, vol. 19, no. 6, p. 597, Dec. 2009.

[22] R. M. May, "Simple mathematical models with very complicated dynamics," *Nature*, vol. 261, no. 5560, pp. 459–467, Jun. 1976.

[23] Z. Jing and J. Yang, "Bifurcation and chaos in discrete-time predator-prey system," *Chaos Soliton Fract.*, vol. 27, no. 1, pp. 259–277, Jan. 2006.

[24] X. Liu and D. Xiao, "Complex dynamic behaviors of a discrete-time predator-prey system," *Chaos Soliton Fract.*, vol. 32, no. 1, pp. 80–94, Apr. 2007.

[25] G. Zhang, Y. Shen, and B. Chen, "Bifurcation analysis in a discrete differential-algebraic predator-prey system," *Appl. Math. Model.*, vol. 38, nos. 19–20, pp. 4835–4848, Oct. 2014.

[26] D. Hu and H. Cao, "Bifurcation and chaos in a discrete-time predator–prey system of Holling and Leslie type," *Commun. Nonlinear Sci.*, vol. 22, nos. 1–3, pp. 702–715, May 2015.

[27] Z. He and X. Lai, "Bifurcation and chaotic behavior of a discrete-time predator–prey system," *Nonlinear Anal., Real World Appl.*, vol. 12, no. 1, pp. 403–417, Feb. 2011.

[28] L. Zhang, C. Zhang, and M. Zhao, "Dynamic complexities in a discrete predator–prey system with lower critical point for the prey," *Math. Comput. Simul.*, vol. 105, pp. 119–131, Nov. 2014.

[29] L. Bai and G. Zhang, "Nontrivial solutions for a nonlinear discrete elliptic equation with periodic boundary conditions," *Appl. Math. Comput.*, vol. 210, no. 2, pp. 321–333, Apr. 2009.

[30] Y. T. Han, G. Zhang, L. Xu, B. Han, L. Zhang, and M. Li, "Turing instability and wave patterns for a symmetric discrete competitive Lotka-Volterra system," *Wseas Trans. Math.*, vol. 10, no. 5, pp. 181–189, May 2011.

[31] D. C. Mistro, L. A. D. Rodrigues, and S. Petrovskii, "Spatiotemporal complexity of biological invasion in a space-and time-discrete predator-prey system with the strong Allee effect," *Ecological Complex.*, vol. 9, p. 32, Feb. 2012.

[32] D. Punithan, D. K. Kim, and R. I. B. McKay, "Spatio-temporal dynamics and quantification of daisy world in two-dimensional coupled map lattices," *Ecological Complex.*, vol. 12, pp. 43–57, Dec. 2012.

[33] L. A. D. Rodrigues, D. C. Mistro, and S. Petrovskii, "Pattern formation in a space-and time-discrete predator–prey system with a strong Allee effect," *Theor. Ecol.*, vol. 5, no. 3, pp. 341–362, Aug. 2012.
[34] F. Zhang, H. Zhang, S. Ma, T. Meng, T. Huang, and H. Yang, "Self-organized patterns induced by Neimark-Sacker, flip and turing bifurcations in a discrete predator-prey model with Lesie-Gower functional response," *Entropy*, vol. 19, no. 6, pp. 1–20, Jun. 2017.

FEIFAN ZHANG is currently with the Engineering Ecology and Nonlinear Science Research Center, North China Electric Power University. He is mainly involved in the formation mechanism research, pattern stability study, entropy, and ecological complexity research in the field of vegetation pattern. He has extensive experience in modeling methods, modeling processes, and model validation.

XUANWEN WU is currently with the School of Mathematics and Physics, North China Electric Power University. His research interests include pattern dynamics, numerical simulations, and the stability of numerical solutions of differential models.

WENJIAO ZHOU is currently with the School of Mathematics and Physics, North China Electric Power University. His research interests include pattern dynamics, numerical solutions of differential models, and bifurcation analysis.

LEI YAO is currently with the School of Mathematics and Physics, North China Electric Power University. His research interests include various bifurcation theories, numerical simulations, and the stability of numerical solutions of differential models.

HUAYONG ZHANG is currently pursuing the Ph.D. degree in biological and environmental engineering with the National University of Tokyo, Japan. He is an Adjunct Professor with Northeast Normal University, and also a Senior Visiting Scholar with Regina University, Canada. He is a Professor and Doctoral Supervisor with the North China Electric Power University, where he is also the Director of the Engineering Ecology and Nonlinear Science Research Center.